Paper

PREDICTION OF FREQUENCY AND EXPOSURE LEVEL OF SOLAR PARTICLE EVENTS

Myung-Hee Y. Kim,* Matthew J. Hayat,*† Alan H. Feiveson,‡ and Francis A. Cucinotta‡

Abstract—**For future space missions outside of the Earth's magnetic field, the risk of radiation exposure from solar particle events (SPEs) during extra-vehicular activities (EVAs) or in lightly shielded vehicles is a major concern when designing radiation protection including determining sufficient shielding requirements for astronauts and hardware. While the expected frequency of SPEs is strongly influenced by solar modulation, SPE occurrences themselves are chaotic in nature. We report on a probabilistic modeling approach, where a cumulative expected occurrence curve of SPEs for a typical solar cycle was formed from a non-homogeneous Poisson process model fitted to a database of proton fluence measurements of SPEs that occurred during the past 5 solar cycles (19–23) and those of large SPEs identified from impulsive nitrate enhancements in polar ice. From the fitted model, we then estimated the expected frequency of SPEs at any given proton fluence threshold with energy >30 MeV (Φ_{30}) during a defined space mission period. Analytic energy spectra of 34 large SPEs observed in the space era were fitted over broad energy ranges extending to GeV, and subsequently used to calculate the distribution of mGy equivalent (mGy-Eq) dose for a typical blood-forming organ (BFO) inside a spacecraft as a function of total Φ_{30} fluence. This distribution was combined with a simulation of SPE events using the Poisson model to estimate the probability of the BFO dose exceeding the NASA 30-d limit of 250 mGy-Eq per 30 d. These results will be useful in implementing probabilistic risk assessment approaches at NASA and guidelines for protection systems for astronauts on future space exploration missions.**

Health Phys. 97(1):68–81; 2009

Key words: analysis, risk; dose, organ; exposure, radiation; radiation, ionizing

INTRODUCTION

THE RISK of radiation-caused cancer and degenerative disease as well as acute radiation syndrome raises major concerns for astronauts' safety during space missions away from the protective zone of low-earth orbit (Cucinotta et al. 2001; Cucinotta and Durante 2006). Galactic cosmic rays (GCRs) produce a predictable background of radiation dose varying about 2-fold in intensity over each (approximately) 11-y solar cycle. On this basis, projections of GCR radiation dose to astronauts for future space missions to the moon and Mars were made from the prediction of long-term behavior (months and years) of the solar cycle, which was developed as an analysis tool for mission design studies (Badhwar et al. 1994; Wilson et al. 1999; Kim and Wilson 2000; Kim et al. 2004, 2006a and b). On the other hand, solar particle events (SPEs) occur quite often and it is difficult to predict their onset and size. Most SPEs would lead to small crew doses even for light spacecraft or shielding, and only a small proportion (about 10%) of individual SPEs would be of concern to astronauts. However, many small events can disrupt mission operations and lead to excessive costs.

For space missions with longer duration, exposure to SPEs with intense particle flux and high energy levels is a major concern, although the risk of early effects may be small due to the reduction of dose-rates behind protective or tissue shielding. There remains a significant cancer risk for some events (Cucinotta 1999; Cucinotta and Durante 2006; Cucinotta et al. 2006). As there are limitations in crew return vehicles and dose limits implemented by the National Aeronautics and Space Administration (NASA) (NCRP 2000), accurate estimation of SPE frequency and its exposure level during a mission period is necessary for protection of astronauts and determining shielding requirements (Cucinotta et al. 2006) for future space missions to the moon and Mars. A probabilistic risk assessment approach is needed to implement the radiation protection requirements from SPEs for astronauts or possible hardware failure, and the model developed in our report will support such efforts.

Other than a general increase in SPE occurrence with increasing solar activity, analysis over recent solar cycles has yielded no recognizable pattern of when

* Universities Space Research Association, Division of Space Life Sciences, 2101 NASA Parkway, SK/SRPE/B37, Houston, TX 77058; † Currently at Johns Hopkins University, Baltimore, MD 21205; ‡ NASA Johnson Space Center, Houston, TX 77058.

For correspondence contact: Myung-Hee Y. Kim, Universities Space Research Association, Division of Space Life Sciences, 2101 NASA Parkway, SK/SRPE/B37, Houston, TX 77058, or email at myung-hee.y.kim@nasa.gov.

(*Manuscript accepted* 18 *February* 2009)
0017-9078/09/0

individual SPEs occur (Goswami et al. 1988; Kim et al. 2005). From this generally recognized characteristic of SPEs, the annual mean frequency of occurrence was represented as a power law function of sunspot number (Nymmik 1999). With the projected sunspot numbers in solar cycle 24, a conservative estimate was made (Kim et al. 2006b) that there would be several occurrences of medium to large SPEs annually in future solar active years (which are typically 2.5 y before and 4.5 y after solar maximum). This estimate was obtained by direct observation of SPE occurrence and annual proton fluences during the active phases in recent 11-y solar activity cycles.

In this study, we used a more comprehensive approach to estimating SPE risk for a specific-term space mission using all available recorded SPE occurrences and proton fluences with energy >30 MeV (Φ_{30}). The database for our analysis was derived from cross calibration of various techniques for measuring proton fluence of all SPEs that were recorded during the space era (1955 to the present). For solar cycles 19–21, the list of major SPEs and their proton fluence assembled by others (King 1974; Feynman et al. 1990; Shea and Smart 1990) contains all the available flux and fluence data in the form of a continuous database. From 1986 to the present (solar cycles 22 and 23), Geostationary Operational Environmental Satellite (GOES; http://goes.ngdc.noaa.gov/data/) spacecraft measurements of the 5-min average integral proton flux for SPEs were obtained through direct access to the National Oceanographic and Atmospheric Agency's (NOAA's) National Geophysical Data Center (NGDC; http://www.ngdc.noaa.gov/stp/SOLAR/getdata.html). In previous work (Kim et al. 2007), the cumulative frequency curve of Φ_{30} event sizes was derived without considering the event onset time. In that study, the probability of one SPE having at least a given size Φ_{30} during a short-term mission was calculated from the normalized cumulative curve multiplied by the occurrence rate assuming independence between event size and occurrence rate.

The probability of multiple events increases with mission period. The sporadic behavior of SPE occurrence is a major operational problem in planning shielding requirements for future lunar and Mars stays in worst-case scenarios during periods of greatest solar activity. To account for the chaotic nature of SPE occurrence, we first estimated a non-homogeneous Poisson process model for explaining the probability distribution of SPE occurrence times. Then, we used the Φ_{30} fluence distribution in the database to predict the expected frequency of large SPEs for an arbitrary mission period. In doing so, we made use of all the SPE data, including those outside the window of interest. We demonstrate that this model-based estimate is considerably more accurate than one based on simple counting of historical events (of which there may be very few) within the window. A goodness-of-fit test was also performed to verify that our model indeed provided a reasonable representation of the data.

Using an analytic representation of energy spectra for 34 historically large SPEs, the Baryon transport code, BRYNTRN (Wilson et al. 1989; Cucinotta et al. 1994), was used to calculate the distribution of mGy equivalent (mGy-Eq) dose at a typical blood-forming organ (BFO) for an astronaut inside a moderately shielded spacecraft. The distribution of mission-specific BFO risk, which is a function of the estimated frequency of SPEs in a given mission period, was then estimated ranging from its 5th to 95th percentile. The results can be useful as a guide for the design of a protection system using probabilistic risk assessment approaches for future space exploration missions.

CUMULATIVE FREQUENCY DISTRIBUTION OF RECORDED SPEs

A total of 370 SPEs were identified during solar cycles 19–23. We found statistically significant differences in the overall distribution of Φ_{30} from cycle to cycle. However, since it is impossible to predict whether a future mission will take place in a cycle similar to any of those on record, fluence data were combined over all 5 cycles to estimate an overall probability distribution of Φ_{30} for an average cycle. Fig. 1 shows sample cumulative tail probabilities of Φ_{30} for cycles 19–23 and the overall cumulative tail probability (thick line). Between the years 1561 and 1950, 71 SPEs with $\Phi_{30} > 2 \times 10^9$ protons cm^{-2} (McCracken et al. 2001) were also identified from impulsive nitrate enhancements in polar ice cores. Applying a correction factor of 4/3 to account for reduced nitrate precipitation during summer and early autumn (McCracken et al. 2001), we estimate that about 95 SPEs with $\Phi_{30} > 2 \times 10^9$ protons cm^{-2} actually occurred during the ice-core sampling period. Assuming the number of SPEs per cycle is about the same for the period represented by the nitrate data as it is for cycles 19–23 (with approximately 700 days of cycle 19 missing), there would have been approximately 2,713 SPEs for the nitrate-data period of which 95 had fluence greater than 2×10^9 protons cm^{-2}. For cycles 19–23, we observed 7 such SPEs out of 370. The proportions 95/2,713 = 0.035 and 7/370 = 0.019 are not significantly different ($p = 0.121$, Fisher's exact test) even with the fairly large sample size of SPEs, thus justifying the combination of corrected nitrate and modern sets of data for estimating the probability of large Φ_{30} values. With

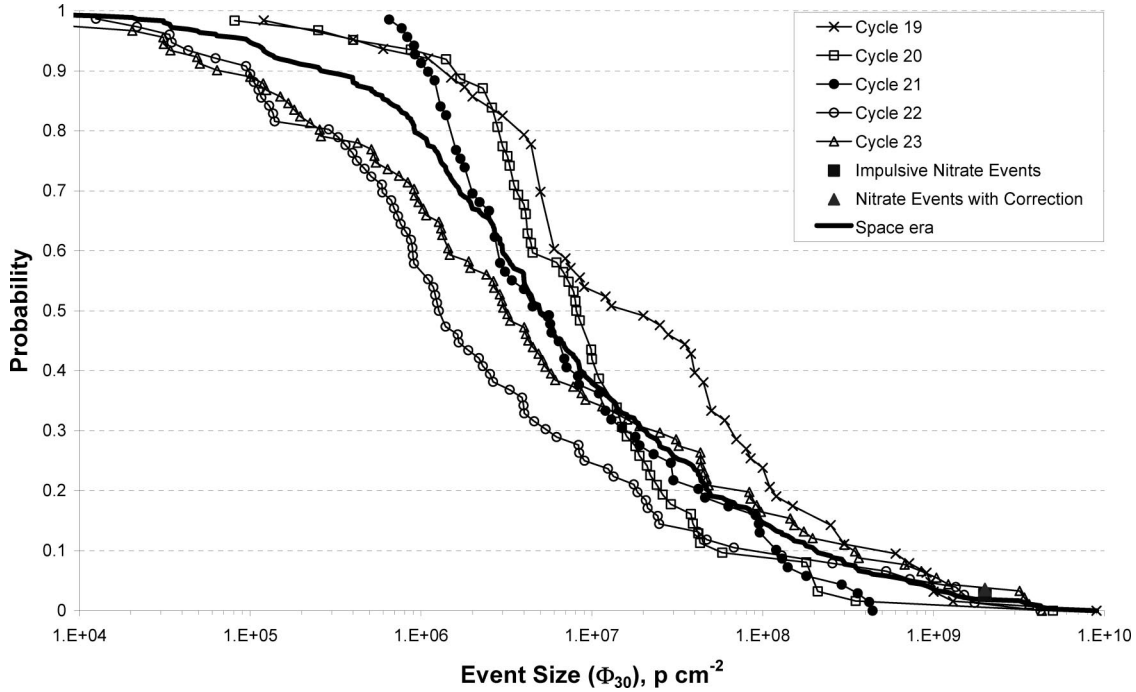

Fig. 1. Probability of an SPE event exceeding the displayed threshold Φ_{30} (combined data of space era is a thick line; data for each cycle is a solid line with a centered symbol; impulsive nitrate events with and without seasonal correction have symbol only displayed).

the combined data an overall estimate of $P(\Phi_{30} > 2 \times 10^9$ protons $cm^{-2}) = (95 + 7)/(2713 + 370) = 0.033$ was obtained. Table 1 summarizes all the available SPE data for the 5 modern cycles and for the nitrate samples.

In an earlier study (Kim et al. 2007), it was assumed that no more than one large SPE could occur over a short mission of 2 wk or less. Under this assumption and also assuming independence between event size and the likelihood of an SPE occurring, the probability of having an SPE with fluence above a given threshold, a, was derived directly:

Table 1. Available SPE database.

Solar Cycle	# of SPE	# of days	Period
Cycle 19	68	3,895	2/1/1954–9/30/1964
Cycle 20	63	4,140	10/1/1964–1/31/1976
Cycle 21	70	3,653	2/1/1976–1/31/1986
Cycle 22	77	3,742	2/1/1986–4/30/1996
Cycle 23	92	4,262	5/1/1996–12/31/2007[a]
Cycles 19–23	370	19,692	2/1/1954–12/31/2007[a]
SPE with $\Phi_{30} \geq 2 \times 10^9$ cm^{-2}	71	Identified from impulsive nitrate enhancements in polar ice between 1561 and 1950	
	7	The 7 large SPEs during space era: Nov 1960 (Cycle 19); Aug 1972 (Cycle 20); Oct 1989 (Cycle 22); July 2000, Nov 2000, Nov 2001, and October 2008 (Cycle 23)	

[a] The end of Cycle 23 estimated.

$$P(\Phi_{30} > a) = P(\Phi_{30} > a|SPE) \times P(SPE). \quad (1)$$

In this earlier study, $P(SPE)$ was estimated conservatively high by counting the number of observed SPEs in a 2-wk window during the period of active phase of a solar cycle, and $P(\Phi_{30} > a|SPE)$ was estimated from the cumulative data shown in Fig. 1.

As mission durations increase, so does the probability of multiple events. Furthermore, missions can occur during any time period within a solar cycle and can also, of course, overlap cycles. Without a model for variable SPE propensity throughout a cycle, using the worst-case scenario can lead to significant errors in planning, resulting in overprotection of astronauts on future missions to the moon and Mars especially in the passive phase of a cycle. The annual mean frequency of SPE occurrence has been estimated using sunspot numbers, as both are likely associated with solar activity phase (Nymmik 1997, 1999). However, even if sunspot number were predictive of SPE propensity, long-range predictive assessment of risk could not use such a model because the sunspot number would be unknown. As an alternative, we used the time within a cycle as an explanatory variable in a model to predict SPE propensity (described in the next section). Not only does this model allow for variable SPE propensity, but it also allows the use of all available data to estimate this propensity, not just data corresponding to a given mission time window.

MODEL-BASED PREDICTION OF SPEs

Poisson model for SPE occurrences

Let $N(t)$ be the number of SPEs occurring from the start of a solar cycle to a time t days later. Then the number of SPEs occurring in an arbitrary time interval (t_1, t_2) is $N(t_2)-N(t_1)$. In developing a probability model for estimating the expected number of SPE occurrences in an arbitrary mission period, we assumed that the values of $N(t)$ follow a non-homogenous Poisson process (Parzen 1967). In other words, the number of events in any time interval is Poisson distributed with mean depending on the end points of the interval, and that the occurrence of an SPE during one time interval does not affect the probability of an SPE occurring in a subsequent interval. This last property, known as "independent increments," allows us to evaluate the statistical likelihood of observing particular "gap" times, i.e., times between successive SPEs, which in turn enables estimation of the expected number of SPEs during a mission.

Hazard function of SPEs

In the Poisson process model, the propensity for SPE occurrence at time t is a continuous function of t, known as the *hazard function*. More formally, the hazard function, $\lambda(t)$, is defined by

$$\lambda(t) = \lim_{h\to 0} \frac{P[SPE_{\text{occurrence}}\,(t, t+h)]}{h}. \qquad (2)$$

In terms of $\lambda(t)$, $E[N(t_1, t_2)]$, the expected number of events in an interval (t_1, t_2), is equal to $m(t_1) - m(t_2)$, where $m(t)$, known as the "mean value function," is the cumulative hazard:

$$m(t) = \int_0^t \lambda(u)du. \qquad (3)$$

The "spikes" in Fig. 2 show the occurrence times of all SPEs in solar cycles 19–23. Because there are typically more SPEs near the middle of cycles than near the beginning and end of cycles, the hazard function should take on relatively low values at the ends of each solar cycle and reach a peak somewhere near the middle of cycles. After studying different models for the hazard function and assessing goodness-of-fit, the functional form best explaining our data was found to be proportional to a beta distribution density function offset by a quantity λ_0; i.e.,

$$\lambda(t) = \frac{\lambda_0}{4{,}000} + \frac{K}{4{,}000}\frac{\Gamma(p+q)}{\Gamma(p)\Gamma(q)} \times \left(\frac{t}{4{,}000}\right)^{p-1}\left(1-\frac{t}{4{,}000}\right)^{q-1} (0 \le t \le 4{,}000), \qquad (4)$$

for a "typical" nonspecific cycle of 4,000-d duration, where λ_0, K, p, and q are parameters to be estimated. After redefining SPE occurrence times relative to 4,000-d cycles and combining across all 5 cycles, we used the method of maximum likelihood to estimate the unknown parameters

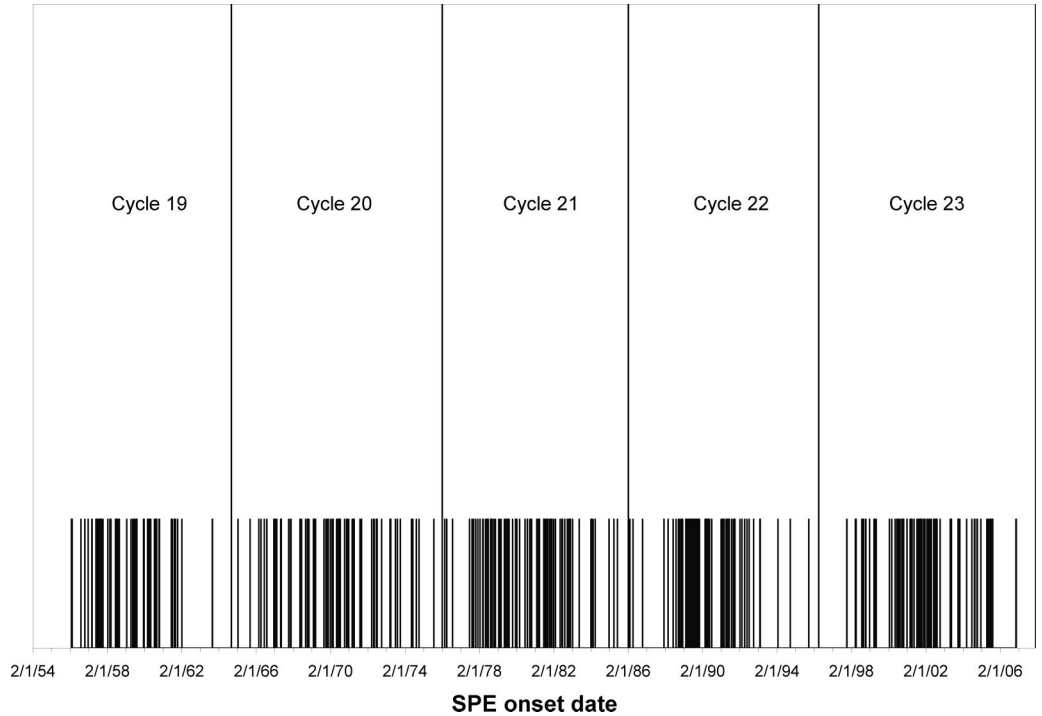

Fig. 2. The onset dates of SPEs occurring between 1 January 1956 and 31 December 2007.

λ_0, K, p, and q. To obtain the likelihood, we used the independent increments property and also the fact that if $N(t)$ follows a Poisson process, the elapsed time between successive SPE events has a particular exponential-type distribution derived from $\lambda(t)$. This distribution would be exactly exponential if $\lambda(t)$ were constant. Resulting maximum-likelihood parameter estimates were $\lambda_0 = 19.52$, $K = 55.89$, $p = 4.073$, and $q = 4.820$. Substitution of these values into eqn (4) for each cycle gives the estimated hazard function, whose units are events per day. In Fig. 3, we have shown this hazard function for the period 1 January 1956 to 31 December 2007, comprising most of cycle 19, and all of cycles 20–23. From eqn (4), it can be shown that μ, the time of peak hazard, is $4{,}000(p-1)/(p+q-2)$ days into a cycle. For the observed data, μ was estimated at 1,783 d.

Goodness-of-fit

With the simplifying assumption that all 5 observed cycles lasted 4,000 d, the relative SPE occurrence times, $t' = (t - t_0)$, where t_0 is the cycle start time, could be superimposed into a combined cycle of 4,000 d with hazard function 5 times $\lambda(t')$ and associated mean value function 5 times $m(t')$. For the combined-cycle data, we have observed $N = 370$ SPEs in the interval $(0, T)$, where $T = 4{,}000$ d. Following the procedure described in Parzen (1967), we tested the hypothesis that SPEs have occurred in accord with a Poisson process with mean value function $5m(t')$. Under our Poisson model with hazard function proportional to an offset beta density, $F(t')$, the cumulative distribution function for the combined relative SPE occurrence times should be equal to

$$F(t) = \frac{5m(t')}{5m(T)} = \frac{m(t')}{m(T)}. \quad (5)$$

Then, the sample cumulative distribution function, $\hat{F}(t')$, for the combined relative occurrence times should be an estimate of $F(t')$. Using the Kolmogorov-Smirnov test, we found that the maximum observed absolute difference between $\hat{F}(t')$ and $F(t')$ was $D = 0.0254$. This value is consistent with our model ($p = 0.966$), therefore supporting the assumption that this model does indeed provided a reasonable representation of the recorded SPE data. Fig. 4 shows a plot of $\hat{F}(t')$ and $F(t')$ for a combined cycle of 4,000 d.

PROBABILITY DISTRIBUTION OF THE NUMBER OF SPEs DURING A MISSION

Expected number of events

Suppose a space mission takes place between times t_1 and t_2 of a solar cycle. Using the basic properties of a

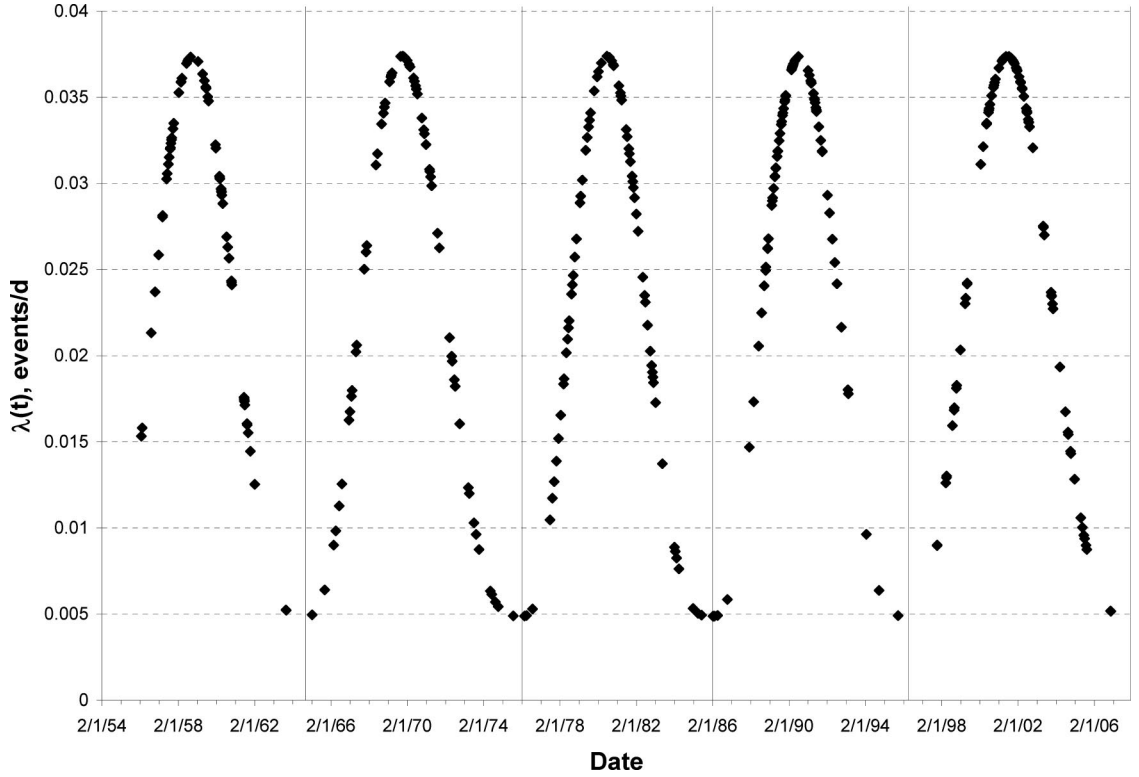

Fig. 3. The estimated hazard function [$\lambda(t)$] for SPEs occurring between 1 January 1956 and 31 December 2007. Each cycle is standardized to a 4,000-d cycle length. Parameters for the hazard function were estimated from the data ($\lambda_0 = 19.52$, $K = 55.89$, $p = 4.073$, and $q = 4.82$).

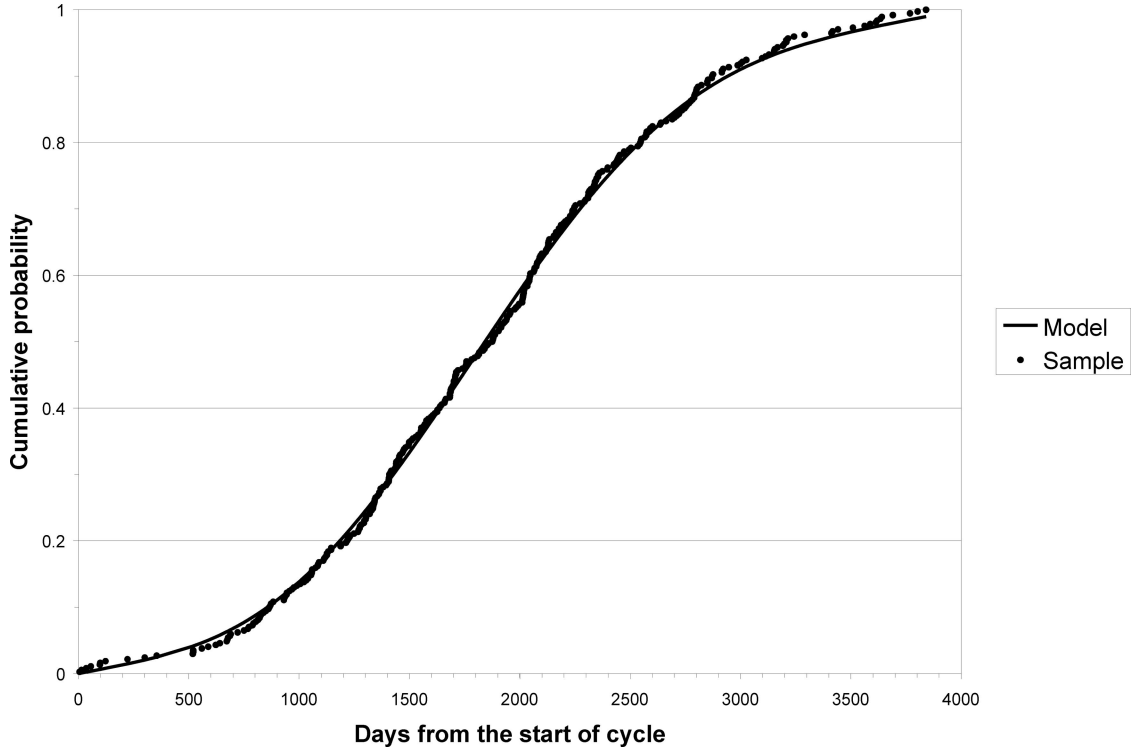

Fig. 4. Comparison of empirical distribution function $\hat{F}(t')$ and the model-based cumulative distribution function $F(t')$ accumulated over 5 cycles, where t' is time (d) relative to the start of a cycle. The Kolmogorov-Smirnov test statistic is the absolute maximum difference of $D = 0.0254$ ($p = 0.966$).

Poisson process, we know $N(t_2) - N(t_1)$, the number of SPEs during the mission, has a Poisson distribution with mean $m(t_2) - m(t_1)$. By using all the SPE occurrence data to first estimate $\lambda(t)$ and then calculate $m(t_2) - m(t_1)$, we are able to obtain a more accurate estimate of the mean rather than by simple counting of cases in the data for which an event occurred in (t_1, t_2).

Number of events with Φ_{30} above a given threshold

If the event size Φ_{30} is independent of $N(t)$, then $N_a(t)$, the number of events up to time t with Φ_{30} exceeding some threshold a is also a Poisson process with hazard function of $q(a)\lambda(t)$, where $q(a) = P(\Phi_{30} > a)$ for an unspecified SPE. To support the independence assumption, Fig. 5 shows a plot of $\log\Phi_{30}$ for each SPE against the log elapsed time (days) between that SPE and the previous one, for solar cycles 19–23. Note that in Fig. 5, there is no evident relationship between elapsed time and Φ_{30}. More formally, 95% confidence limits for Somers' D, a non-parametric measure of association (Newson 2006), were $(-0.058, 0.077)$ with the point estimate being not significantly different from zero ($p = 0.78$).

Independence between the number and size of events allows us to estimate the mean number of events of a given size in an arbitrary period of time. Let $T_0, T_1, \ldots, T_n$ denote the SPE occurrence times over the 5 cycles and let the elapsed time between two consecutive events be $d_i = T_i - T_{i-1}$. Then $N(t) = k$ if and only if

$$\sum_{i=1}^{k} d_i \le t$$

and

$$\sum_{i=1}^{k+1} d_i > t.$$

In other words, $N(t)$ is completely defined in terms of the d_i. It follows that if Φ_{30} is independent of elapsed time, so must Φ_{30} be independent of $N(t)$. We therefore estimated the mean number of "large" ($\Phi_{30} > a$) events in a mission over the period t_1 to t_2 by

$$\hat{E}(a;t_1,t_2) = \hat{q}(a)[\hat{m}(t_1) - \hat{m}(t_2)], \qquad (6)$$

for $a = 10^7$, 10^8, and 2×10^9 p cm^{-2}. In eqn (6), $\hat{q}(a)$ denotes the estimate of $q(a)$ obtained by direct count from the 5-cycle data in Table 1 for $a = 10^7$ and 10^8; and by the combined nitrate and space-era data for $a = 2 \times 10^9$. Also in eqn (6), $\hat{m}(t_1)$ and $\hat{m}(t_2)$ were obtained by integration of the estimated hazard function described by

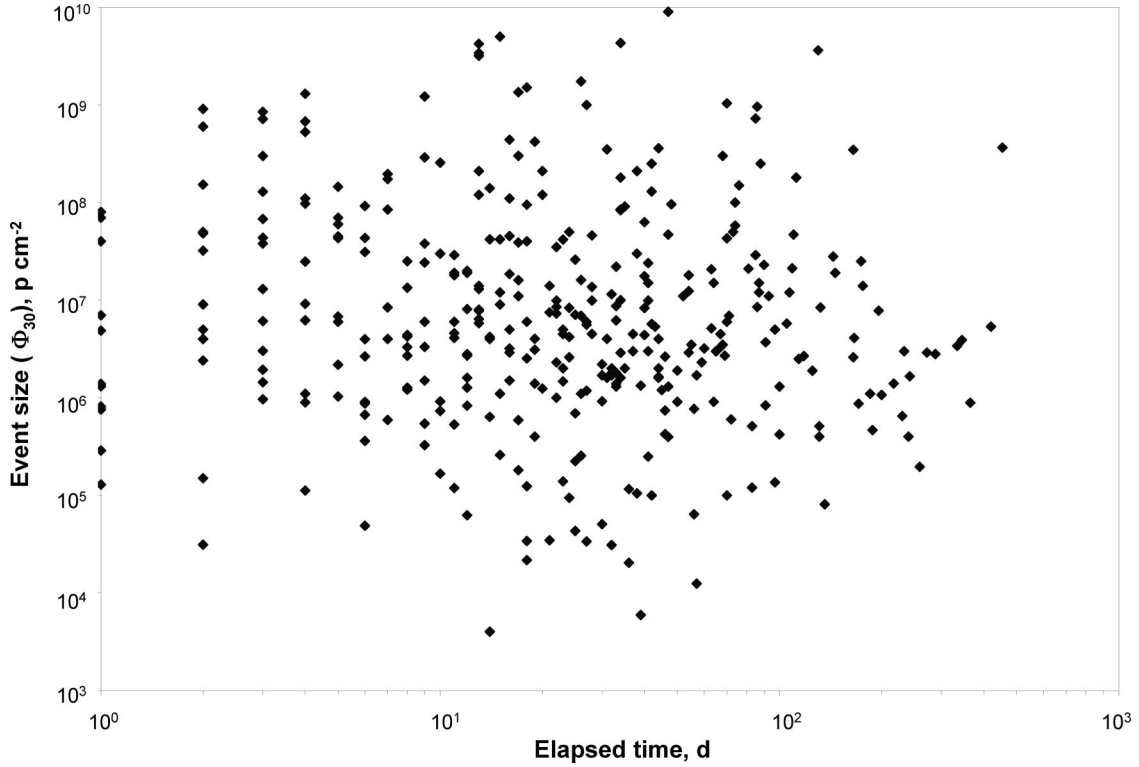

Fig. 5. Event sizes are plotted against the time between events for 370 recorded SPEs. The random nature of the scatter plot suggests independence between event frequency and severity.

eqn (4). Counts of SPEs with $\Phi_{30} > a$, and resulting values of $\hat{q}(a)$ with standard errors in parentheses are shown in Table 2. Table 3 shows $\hat{E}(a;t_1,t_2)$ for values of a above, and for missions of lengths 120, 180, 240, 360, and 540 d. For conservatism, missions were assumed to take place centered on the time of greatest hazard, μ = 1,783 d into a solar cycle, so that $t_1 = 1{,}783 - d/2$ and $t_2 = 1{,}783 + d/2$, where d is mission length (days). In columns 6–7 of Table 3 ("window-based"), estimates of $\hat{E}(a;t_1,t_2)$ were made only from SPEs observed between t_1 and t_2, whereas in columns 8–9 ("model-based"), the entire data set of SPEs was used to form a model-based estimate of $\hat{E}(a;t_1,t_2)$. Note that the standard error of the model-based estimate is much smaller than that of the window-based estimate, illustrating the improved accuracy. Values of $\hat{E}(a;t_1,t_2)$ for a continuous range of thresholds and mission lengths were obtained by interpolation and extrapolation of the data in Table 3. The resulting contour map is shown in Fig. 6.

Table 2. Large SPE data and estimated probability for an unspecified SPE exceeding a, $\hat{q}(a)$.

a, p cm^{-2}	# SPE exceeding a	Total SPE	$\hat{q}(a)$ and (standard error)
10^7	137	370	0.376 (0.0252)
10^8	53	370	0.146 (0.0184)
2×10^9 (space era)	7	370	—
2×10^9 (corrected nitrate data)	95	3,402	—
2×10^9 (combined)	102	3,772	0.029 (0.0033)

Cumulative probability of SPE occurrence during a given mission period

In addition to knowing the expected number of SPEs of a given size within a mission period, the actual distribution of $N_a(t_2) - N_a(t_1)$, the numbers of such events, provides useful information for mission planning. Using the fitted Poisson model, the estimated cumulative probability distributions of $N_a(t_2) - N_a(t_1)$ have been plotted in Fig. 7 for missions centered at μ, with the same lengths and Φ_{30} thresholds ("a") as in Table 3. For example, in Fig. 7a, for a 120-d mission the probability of at least one "large" SPE (Φ_{30} fluence greater than 10^7 protons cm^{-2}) is about 0.8 (80%), with the probability of having at least two large SPEs about 50%, about 20% for more than two SPEs, etc. As mission durations reach 540 d, there is almost no chance of avoiding an SPE whose event size is greater than 10^7 protons cm^{-2}. These figures show that the probability for the multiple numbers of SPE occurrences is increased for longer missions and decreased for higher thresholds.

Table 3. Estimation of number of events, $\hat{E}_a$, for a given threshold and mission period.

# days	t		Estimate of μ	a, p/cm^2	Mission data (window-only)		Model-based (all data)	
	t_1	t_2			Predicted events frequency	Standard error	Predicted events frequency	Standard error
120	1,723	1,843	1,783	10^7	0.90	0.59	1.68	0.17
				10^8	0.35	0.23	0.65	0.10
				10^9	0.08	0.06	0.16	0.04
				[a]2×10^9	0.07	0.05	0.13	0.02
180	1,693	1,873	1,783	10^7	2.18	0.92	2.52	0.25
				10^8	0.85	0.37	0.98	0.14
				10^9	0.20	0.10	0.24	0.07
				[a]2×10^9	0.17	0.07	0.20	0.03
240	1,663	1,903	1,783	10^7	3.16	1.11	3.36	0.33
				10^8	1.23	0.45	1.30	0.19
				10^9	0.30	0.13	0.31	0.09
				[a]2×10^9	0.25	0.09	0.26	0.04
360	1,603	1,963	1,783	10^7	3.98	1.25	5.02	0.49
				10^8	1.55	0.52	1.95	0.28
				10^9	0.37	0.16	0.47	0.13
				[a]2×10^9	0.31	0.10	0.39	0.05
540	1,513	2,053	1,783	10^7	6.01	1.56	7.45	0.73
				10^8	2.34	0.66	2.89	0.42
				10^9	0.56	0.21	0.70	0.20
				[a]2×10^9	0.47	0.13	0.58	0.08

[a] Impulsive nitrate data included.

ORGAN DOSE ASSESSMENT FROM SPE EXPOSURE

The preceding analysis estimates the distribution of the number of SPEs exceeding an event size of Φ_{30} in a given mission period. However, to plan shielding requirements for future space missions, it is useful to have an estimate of the biologically relevant doses of SPEs. To do this we used a Monte Carlo simulation to estimate the overall probability distribution of SPE-attributable mGy-Eq dose (NCRP 2000) at a generic BFO of an astronaut in a nominally shielded spacecraft. The simulation took into account not only the randomness of SPEs and event sizes, but also the variation of energy spectra for the SPEs.

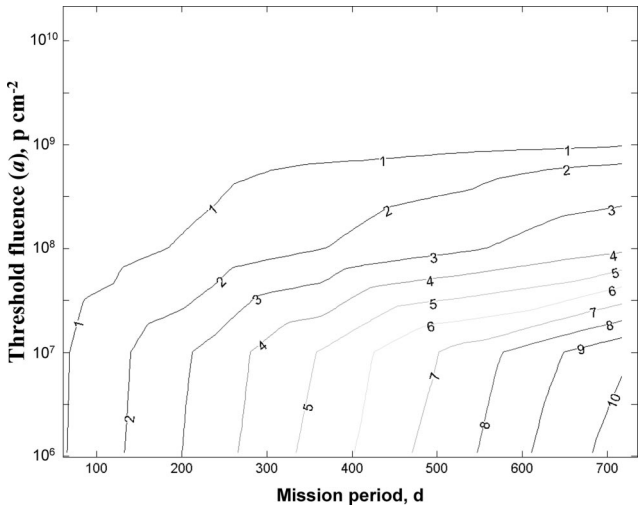

Fig. 6. Contours of equal expected numbers of SPEs with Φ_{30} fluence exceeding a for various combinations of a and mission length.

To accomplish this, we first considered 34 historically large SPEs recorded in the space era for the estimation of individual exposure levels in interplanetary space. For each SPE, $\Phi(>E)$, the event-integrated fluence above an arbitrary energy level of E MeV was approximated by the Weibull model:

$$\Phi(>E) = P_0 e^{-aE^b}, \tag{7}$$

where P_0 is the total integrated fluence. Observed values of $\Phi(>30$ MeV) and the parameters P_0, a and b were estimated by fitting the observed spectra at discrete energy levels, and are listed in Table 4.

Using eqn (7), each of the 34 energy spectra was extended over broad energy ranges out to 1 GeV, and then propagated through the spacecraft and body tissue using the Baryon transport code, BRYNTRN (Wilson et al. 1989; Cucinotta et al. 1994). This code includes the transport of high-energy light ions including neutrons with atomic number $Z \leq 2$ (n, p, d, t, h, and α) and solves the fundamental Boltzmann transport equation. Doses for heavy ion target fragments with $Z > 2$ produced in shielding or tissue are also estimated using a local energy deposition model (Wilson et al. 1991). With the straight-ahead approximation, the transport equation is written as (Wilson et al. 1991):

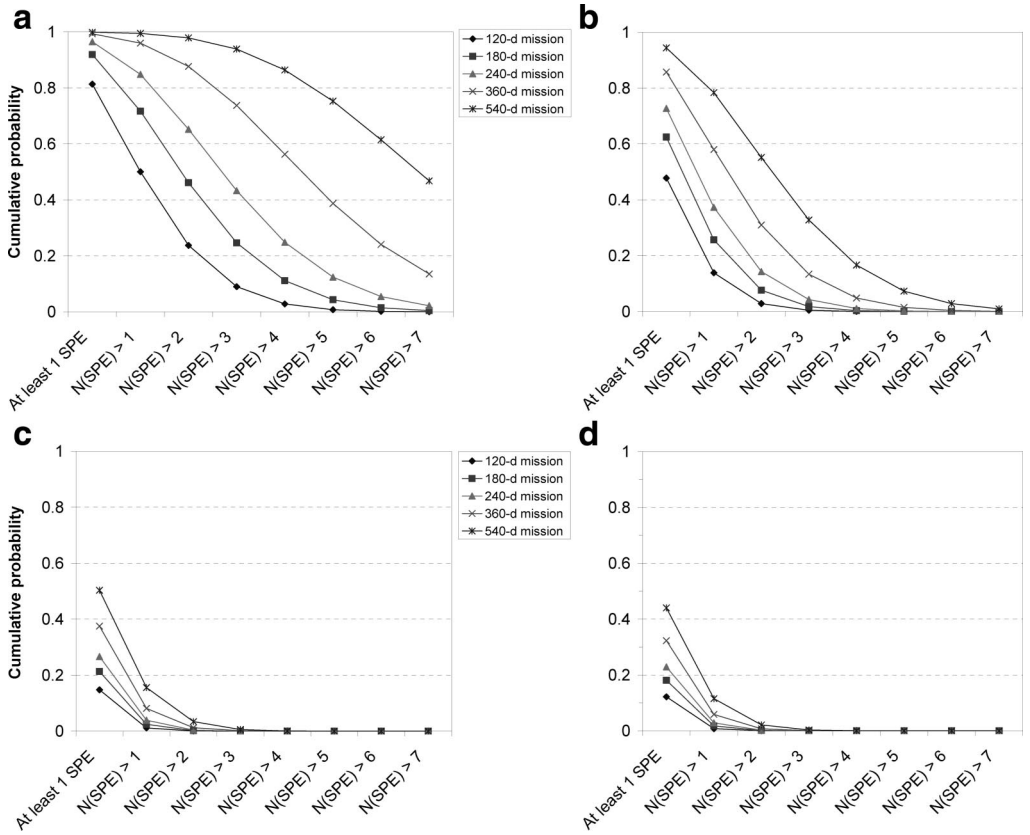

Fig. 7. The cumulative probability of a given number of SPE events exceeding a specified threshold during missions of various lengths are displayed in figures (a–d). The event thresholds considered are: (a) $\Phi_{30} > 10^7$ protons cm^{-2}; (b) $\Phi_{30} > 10^8$ protons cm^{-2}; (c) $\Phi_{30} > 10^9$ protons cm^{-2}; and (d) $\Phi_{30} > 2 \times 10^9$ protons cm^{-2}.

$$\left[\frac{\partial}{\partial x} - \frac{\partial}{\partial E}\tilde{S}_j(E) + \sigma_j(E)\right]\phi_j(x, E) = \sum_{k \geq j}\int_E^\infty \sigma_{jk}(E, E')\phi_k(x, E')dE', \quad (8)$$

where

$\phi_j(x,E)$ = flux of ions of type j with atomic mass A_j having energy E at spatial location x, (MeV^{-1} amu cm^{-2});
σ_j = macroscopic total nuclear-absorption cross sections (cm^2 g^{-1});
$\tilde{S}_j$ = change in E per unit distance, scaled from proton stopping power (MeV amu^{-1} cm^2 g^{-1}); and
σ_{jk} = differential nuclear-interaction cross sections (cm^2 g^{-1} MeV^{-1} amu).

To evaluate the flux of particles of type j with energy E, the input database required consists of the stopping power, the macroscopic total nuclear cross sections, and the differential nuclear-interaction cross sections. The differential cross sections σ_{jk} describe the production of type j particles with energy E by type k particles of energies $E' > E$. These data are those compiled for the present BRYNTRN code (Cucinotta et al. 1994; Wilson et al. 1989).

The absorbed dose D due to energy deposition at a given location x by all particles is calculated with $S_j(E)$, which is the change in E per unit distance for the ions of type j (MeV amu^{-1} cm^2 g^{-1}),

$$D(x) = \sum_j \int_0^\infty S_j(E)\phi_j(x, E)dE. \quad (9)$$

For human exposure, the dose-equivalent is defined by the quality factor Q, which relates the biological damage incurred from any ionizing radiation to the damage produced by γ rays. In general, Q is a function of linear energy transfer which depends on both particle type and energy. For dose-equivalent calculations, the quality factors used are those defined by the International Commission on Radiological Protection Publication 60 (ICRP 1991). The values of dose-equivalent H are computed at a given location x by all particles according to

Table 4. Weibull distribution spectral parameters of $\Phi(>E) = P_0 e^{-aE^b}$.

SPE	$\Phi(>30$ MeV), protons cm^{-2}	P_0	a	b
11/12/1960	9.00×10^9	7.54×10^{10}	0.1279	0.8264
8/2/1972	8.10×10^9	4.58×10^{10}	0.1172	0.7879
10/19/1989	4.23×10^9	1.91×10^{12}	2.5677	0.256
7/14/2000	3.74×10^9	8.23×10^{10}	0.5203	0.5346
10/26/2003	3.25×10^9	7.81×10^{10}	0.5172	0.5425
11/4/2001	2.92×10^9	8.25×10^{10}	0.5241	0.5531
11/8/2000	2.27×10^9	2.30×10^{10}	0.2947	0.6131
3/23/1991	1.74×10^9	4.07×10^{10}	0.2569	0.7418
8/12/1989	1.51×10^9	8.43×10^{10}	0.7304	0.508
9/29/1989	1.35×10^9	1.90×10^{10}	0.5493	0.4643
7/14/1959	1.30×10^9	1.88×10^{12}	3.1025	0.2507
1/16/2005	1.04×10^9	4.15×10^{10}	0.9557	0.4033
2/23/1956	1.00×10^9	4.87×10^9	0.3758	0.4227
7/10/1959	1.00×10^9	2.49×10^{11}	2.061	0.2896
5/10/1959	9.60×10^8	5.44×10^{12}	4.2978	0.2054
7/16/1959	9.10×10^8	1.22×10^{11}	1.9011	0.278
9/24/2001	8.02×10^8	5.13×10^{10}	0.8366	0.4766
10/30/1992	7.27×10^8	8.32×10^{10}	1.3079	0.3827
11/15/1960	7.20×10^8	1.67×10^{11}	2.4367	0.2363
11/22/2001	7.15×10^8	6.02×10^{10}	0.5794	0.6067
6/4/1991	5.28×10^8	2.25×10^{10}	0.8798	0.4279
1/24/1971	3.50×10^8	7.44×10^9	0.3833	0.616
4/20/1998	3.47×10^8	7.07×10^9	0.2758	0.7155
7/18/1961	3.00×10^8	1.13×10^{10}	1.044	0.3666
4/21/2002	2.72×10^8	1.56×10^9	0.1341	0.767
11/2/1969	2.60×10^8	2.68×10^9	0.3124	0.573
6/14/1991	2.56×10^8	3.48×10^{10}	1.6219	0.329
3/23/1958	2.50×10^8	4.19×10^{11}	2.6832	0.2992
7/7/1958	2.50×10^8	9.00×10^{10}	1.6613	0.3719
11/18/1968	2.10×10^8	5.24×10^9	0.4452	0.5617
4/11/1969	2.10×10^8	9.43×10^{10}	1.5538	0.3908
11/6/1997	1.53×10^8	5.40×10^9	1.1301	0.34
11/2/2003	1.50×10^8	5.25×10^{10}	2.0634	0.3112
11/30/1989	1.29×10^8	9.38×10^{10}	1.1566	0.5126

$$H(x) = \sum_j \int_0^\infty Q_j(E) S_j(E) \phi_j(x, E) dE. \quad (10)$$

For the deterministic acute effects, the quality factors for the dose-equivalent generally overestimates the relative biological effectiveness (RBE), and the National Council for Radiological Protection (NCRP 2000) has recommended that risks for non-cancer or deterministic effects be made in terms of an alternate dose quantity Gy-Eq using radiation field-dependent RBE for specific components, because distinct radiation quality functions occur for acute radiation risks and cancer. For the estimation of deterministic acute effects from an intense SPE on lunar or Mars missions during transition and on surface, the new dosimetric quantity of Gy-Eq (G_T) was implemented using the NCRP's RBE and the suggested definition of neutron RBE (Wilson et al. 2002) for a full definition of neutron RBE, and it is defined as

$$G_T = RBE_j \times D_T, \quad (11)$$

where RBE_j is a recommended value for RBE for deterministic effects for a given particle type j on the body, and D_T is the mean absorbed dose in an organ or tissue. Table 5 shows the RBE as given by NCRP and the suggested RBE values for neutron fields.

Organ dose assessment at a specific anatomical location is calculated with the point particle fluxes for given number of rays that traverse various media, such as spacecraft, equipment, tissue equivalent material, and any other media in the path of the ray. Each separate medium's thickness distribution along a ray surrounding a specific organ at a specific position inside spacecraft can be generated using the NASA developed ray tracing model based the CAD tool, ProE (Ponomarev et al. 2007), which uses an evenly spaced distribution of the given number of rays over a 4π solid angle. In the current study, a typical shield configuration was approximated as a spherical structure of 5 g cm^{-2} aluminum for the equipment room of a spacecraft. For the astronaut's organ dose assessment at the BFO, the human body geometry is based on the 50th percentile United States Air Force male in the standing position used by the Computerized Anatomical Man (CAM) model (Billings and Yucker 1973).

For the large SPEs in Table 4, the values of log Φ_{30}, and corresponding observed spectral characteristics, calculated exposure levels at a typical BFO are shown as filled squares in Fig. 8. These data appear to be approximately modeled by a linear trend on a log-log scale, included as a solid line in the figure. Based on the linear fit with an assumed Gaussian distribution of dose around the regression line attributable to variability of spectra, vertical lines represent a range from the 5th to the 95th percentiles of the distribution of BFO dose for future SPEs as a function of Φ_{30}. Included in the figure is the current NASA 30-d limit (NRC/NAS 2008) of 250 mGy-Eq at a BFO (horizontal dashed line). Using the

Table 5. Particle RBE (NCRP 2000) and the RBE for neutrons suggested by Wilson et al. (2002) for deterministic effects.

Particle type	RBE value	
	NCRP	Suggested by Wilson et al. (2002)
Less than 1 MeV neutrons	RBE (fission neutrons)	5.0
1 to 5 MeV neutrons	6.0	
5 to 50 MeV neutrons	3.5	
Above 25 MeV neutrons	RBE (not more than those of 1–25 MeV neutrons)	3.5
Protons >2 MeV	1.5	
Heavy ions (helium, carbon, neon, argon)	2.5	
Heavy ions, all others	2.5	

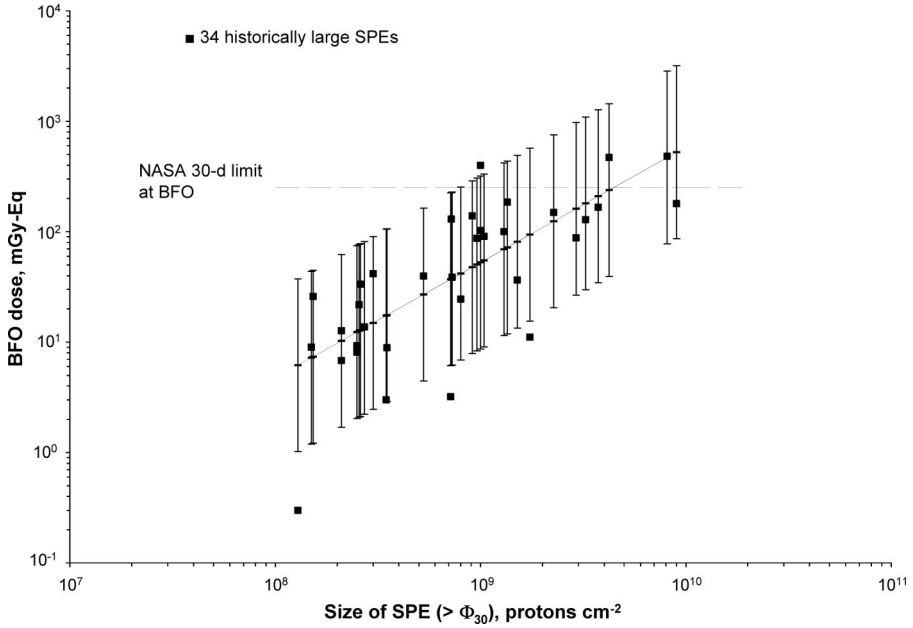

Fig. 8. BFO dose vs. Φ_{30} fluence for 34 historically large SPEs. The best linear fit regression line is shown, along with 90% tolerance limits.

fitted regression model, the probability of exceeding the NASA 30-d dose limit was calculated as a function of Φ_{30} and shown in Fig. 9. For example, it can be seen that the dose absorbed by a BFO in an equipment room in interplanetary space has about a 20% chance of exceeding the current NASA 30-d limit for a future SPE with $\Phi_{30} = 2 \times 10^9$ protons cm^{-2}. During the space era, 7 large SPEs have been observed with event-integrated fluence above 2×10^9 protons cm^{-2}. From Fig. 9, it can be seen that, for similar SPEs in the future, the probabilities of the dose at a BFO exceeding the above NASA 30-d limit range from 0.25 ($\Phi_{30} = 2.27 \times 10^9$) to 0.73 ($\Phi_{30} = 9.0 \times 10^9$) for a vehicle with shielding of 5 g cm^{-2} of aluminum in interplanetary space.

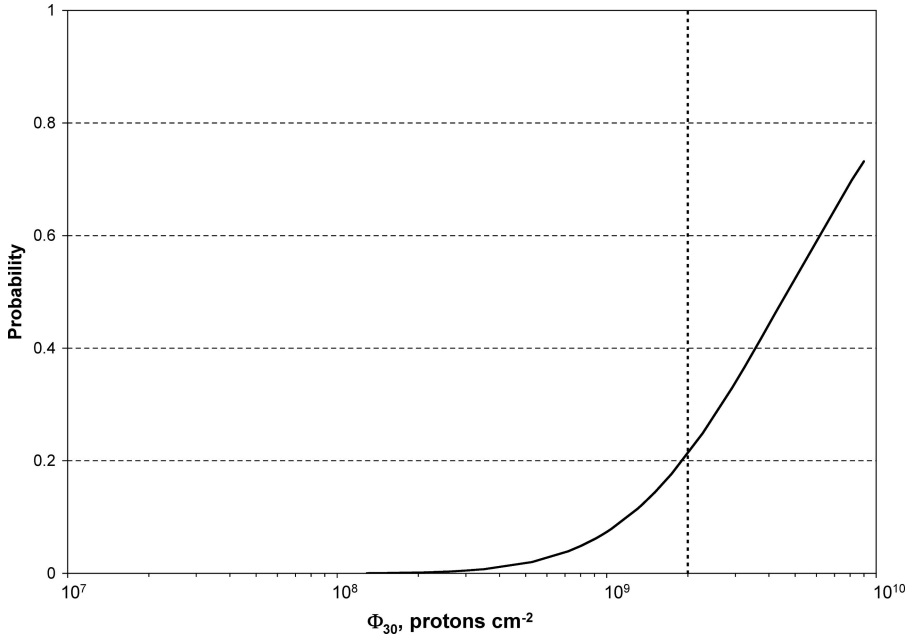

Fig. 9. Probability of exceeding the NASA 30-d limit of BFO dose for a given fluence level inside a spacecraft of 5 g cm^{-2} aluminum in interplanetary space exposed from various SPE event size.

In actuality, with the same shielding configuration, the BFO dose from the largest event recorded in the space era ($\Phi_{30} = 9.0 \times 10^9$) was lower than the NASA 30-d BFO dose limit, but doses for three smaller events ($\Phi_{30} = 1.00 \times 10^9$, $\Phi_{30} = 4.23 \times 10^9$, and $\Phi_{30} = 8.10 \times 10^9$) were over the limit. These results demonstrate that in addition to the total fluence, the variable shape of the energy spectrum for each SPE is an extremely important factor for the total exposure calculation and must be considered along with a measure of the integral event fluence. Energy spectra for the nitrate events are not known. However, Reames and Ng (1998) have described a so-called "streaming limit" that reduces the possibility of SPE energy spectra with higher energies than those observed in the space era.

An empirical distribution of BFO dose for a range of potential mission lengths was obtained with Monte Carlo simulation, using random draws from the estimated distributions of BFO dose given Φ_{30}, the number of SPEs, and the Φ_{30} event size. The latter was simulated using a gamma distribution model for the distribution of $\log_{10} \Phi_{30}$. As previously, the conservative assumption that all missions were centered at the time of maximum SPE activity was made. The results, illustrated in Fig. 10, show various percentiles of BFO dose plotted against mission length. Dose-rate was not considered in the present analysis, however it will be studied in future work. The additional consideration of organ dose-rate will be needed to consider models of acute radiation syndromes and cancer risks as these risks are highly dependent on the dose-rate (NCRP 2000).

CONCLUSION

For the sporadic nature of SPE occurrences, the probabilities of SPEs occurring in a given mission period

Estimate of number of events for a given threshold

# Days	t t_1	t t_2	Estimate of μ	a, p/cm^2	Mission data [window-only] Predicted events frequency	Mission data [window-only] Standard Error	Model-based [all data] Predicted events frequency	Model-based [all data] Standard Error
120	1723	1843	1783	10^7	0.90	0.59	1.68	0.17
				10^8	0.35	0.23	0.65	0.10
				10^9	0.08	0.06	0.16	0.04
				2×10^9	0.07	0.05	0.13	0.02

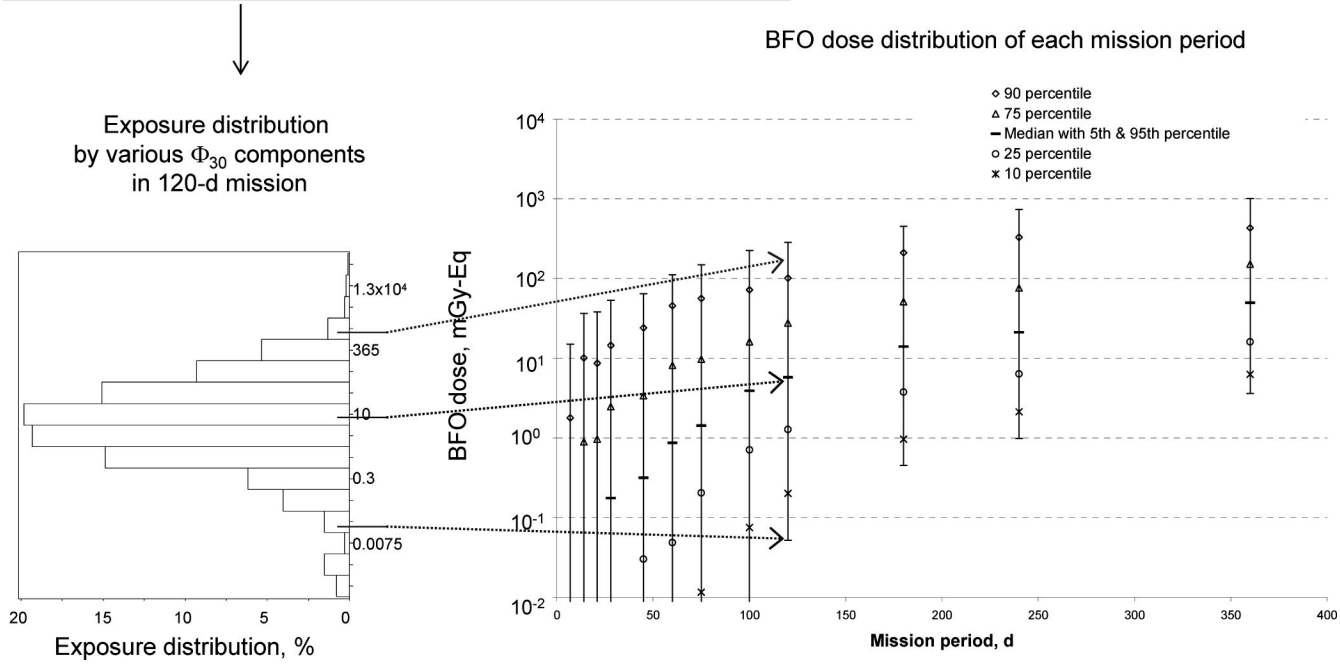

Fig. 10. Results of the simulation incorporating three stages of modeling for a given mission are displayed: (1) The number of SPEs for a 120-d mission, as an example, is simulated by random draws from a Poisson distribution model with mean $m(t_2) - m(t_1)$; (2) For each event occurrence, its Φ_{30} fluence is simulated with a random draw from a gamma distribution; (3) For each event and corresponding fluence, the log BFO dose is simulated by a draw from a normal distribution about the regression line in Fig. 8. Results for various mission lengths, including those for a 120-d mission pointed by arrows, are displayed.

were estimated by employing a probabilistic modeling approach. The cumulative frequency distribution of recorded SPEs was formed using the combined database of proton fluence measurements of SPEs that have occurred during the past 5 solar cycles and those of large proton SPEs that were identified from impulsive nitrate enhancements in polar ice. In previous work, the probability of an SPE at a given threshold event size was conservatively estimated for a short mission, such as one or two weeks, assuming conservatively that the mission would occur during time of maximum solar activity. In a more realistic analysis, the frequency of SPE occurrences in an arbitrary mission period was estimated from a non-homogenous Poisson process model, which applies a non-constant hazard function to account for the rise and fall of SPE propensity during a typical solar cycle. The resultant cumulative distribution function of SPE occurrence times was compared with recorded SPE data during the past 5 solar cycles using the Kologomorov-Sirnov goodness-of-fit test. The result showed that the current model provided a very reasonable representation of the non-constant SPE occurrence propensity throughout a cycle. Assuming independence between SPE threshold fluences and occurrence times, we then used the model to estimate the expected frequency of SPEs above particular certain threshold fluence levels in an arbitrary mission period. To estimate the biological impact of SPEs, 34 historically large SPEs were analyzed by modeling the analytic energy spectra of each event from the proton fluence measurements. Representative SPE-caused BFO exposure levels and their variability were then estimated as a function of the size of the SPE. This enabled us to calculate predicted percentiles of BFO exposure levels that would be expected during a given mission period. The results will be used in developing guidelines for protection systems for astronauts during future space exploration missions.

Acknowledgments—This work was supported in part by the NASA Space Radiation Risk Assessment Project, and the Living with Star Program's Earth-Moon-Mars Radiation Exposure Module (EMMREM) support at NASA Johnson Space Center.

REFERENCES

Badhwar GB, Cucinotta FA, O'Neill PM. An analysis of interplanetary space radiation exposure for various solar cycles. Radiat Res 138:201–208; 1994.

Billings MP, Yucker WR. The computerized anatomical man (CAM) model. Washington, DC: NASA; CR-134043; 1973.

Cucinotta FA. Issues in risk assessment from solar particle events. Radiat Meas 30:261–268; 1999.

Cucinotta FA, Durante M. Cancer risk from exposure to galactic cosmic rays: implications for space exploration by human beings. Lancet Oncol 7:431–435; 2006.

Cucinotta FA, Wilson JW, Badavi FF. Extension to the BRYNTRN code to monoenergetic light ion beams. Washington, DC: NASA; Report No. TP-3472; 1994.

Cucinotta FA, Schimmerling W, Wilson JW, Peterson LE, Saganti P, Badhwar GD, Dicello JF. Space radiation cancer risks and uncertainties for Mars missions. Radiat Res 156:682–688; 2001.

Cucinotta FA, Kim MH, Ren L. Evaluating shielding effectiveness for reducing space radiation cancer risks. Radiat Meas 41:1173–1185; 2006.

Feynman J, Armstrong T, Dao-Gibner L, Silverman SJ. Spacecraft 27:403–410; 1990.

Goswami JN, McGuire RE, Reedy RC, Lal D, Jha R. Solar flare protons and alpha particles during the last three solar cycles. J Geophys Res 93:7195–7205; 1988.

International Commission on Radiobiological Protection. 1990 recommendations of the International Commission on Radiobiological Protection. New York: Elsevier Science; ICRP Publication 60; Ann ICRP 21/1–3; 1991.

Kim MY, Wilson JW. Examination of solar cycle statistical model and new prediction of solar cycle 23. Washington, DC: NASA; Report No. TP-2000-210536; 2000.

Kim MY, Wilson JW, Cucinotta FA. An improved solar cycle statistical model for the projection of near future sunspot cycles. Washington DC: NASA; Report No. TP-2004-212070; 2004.

Kim MY, Hu X, Cucinotta FA. Effect of shielding materials from SPEs on the lunar and Mars surface. Reston, VA: American Institute of Aeronautics and Astronautics; paper number AIAA 2005-6653; 2005.

Kim MY, Wilson JW, Cucinotta FA. A solar cycle statistical model for the projection of space radiation environment. Adv Space Res 37:1741–1748; 2006a.

Kim MY, Cucinotta FA, Wilson JW. Mean occurrence frequency and temporal risk analysis of solar particle events. Radiat Meas 41:1115–1122; 2006b.

Kim MY, Cucinotta FA, Wilson JW. A temporal forecast of radiation environments for future space exploration missions. Radiat Environ Biophys 46:95–100; 2007.

King JH. Solar proton fluences for 1977–1983 space missions. J Spacecraft 11:401–408; 1974.

McCracken KG, Dreschhoff GAM, Zeller EJ, Smart DF, Shea MA. Solar cosmic ray events for the period 1561–1994. 1. Identification in polar ice, 1561–1950. J Geophys Res 106:21585–21598; 2001.

National Council on Radiation Protection and Measurements. Radiation protection guidance for activities in low-Earth orbit. Bethesda, MD: National Council on Radiation Protection and Measurements; NCRP Report No. 132; 2000.

National Research Council/National Academy of Sciences, Committee on the Evaluation of Radiation Shielding for Space Exploration. Managing space radiation risk in the new era of space exploration. Washington, DC: National Academies Press; 2008.

Newson R. Confidence intervals for rank statistics: Somers D and extensions. The Stata J 6:309–334; 2006.

Nymmik RA. Dependence of the rate of events of solar cosmic rays on solar activity level. Cosmic Res 35:213–215; 1997.

Nymmik RA. Probabilistic model for fluences and peak fluxes of solar energetic particles. Radiat Meas 30:287–296; 1999.

Parzen EJ. Stochastic processes. San Francisco: Holden-Day, Inc; 1967.

Ponomarev AL, Nounu HN, Hussein HF, Kim MY, Atwell W, Cucinotta FA. NASA-developed ProE-based tool for the ray-tracing of spacecraft geometry to determine radiation doses and particle fluxes in habitable areas of spacecraft and

in the human body. Washington, DC: NASA; Report No. TP-2007-214770; 2007.
Reames DV, Ng CK. Streaming-limited intensities of solar energetic particles. Astrophys J 504:1002–1005; 1998.
Shea MA, Smart DF. A summary of major proton events. Solar Phys 127:297–320; 1990.
Wilson JW, Townsend LW, Nealy JE, Chun SY, Hong BS, Buck WW, Lamkin SL, Ganapole BD, Kahn F, Cucinotta FA. BRYNTRN: a Baryon transport model. Washington, DC: NASA; Report No. TP-2887; 1989.
Wilson JW, Townsend LW, Schimmerling W, Khandelwal GS, Khan F, Nealy JE, Cucinotta FA, Simonsen LC, Shinn JL, Norbury JW. Transport methods and interactions for space radiations. Washington, DC: NASA; Report No. RP-1257; 1991.
Wilson JW, Kim MY, Shinn JL, Tai H, Cucinotta FA, Badhwar GD, Badavi FF, Atwell W. Solar cycle variation and application to the space radiation environment. Washington, DC: NASA; Report No. TP-1999-209369; 1999.
Wilson JW, Kim MY, De Angelis G, Cucinotta FA, Yoshizawa N, Badavi FF. Implementation of Gy-Eq for deterministic effects limitation in shield design. J Radiat Res 43:S103–S106; 2002.

■ ■